

4S-DT: Self Supervised Super Sample Decomposition for Transfer learning with application to COVID-19 detection

Asmaa Abbas¹, Mohammed M. Abdelsamea^{1,2,*}, and Mohamed Medhat Gaber²

¹Mathematics Department, University of Assiut, Assiut, Egypt

²School of Computing and Digital Technology, Birmingham City University, Birmingham, UK

*mohammed.abdelsamea@bcu.ac.uk

ABSTRACT

Due to the high availability of large-scale annotated image datasets, knowledge transfer from pre-trained models showed outstanding performance in medical image classification. However, building a robust image classification model for datasets with data irregularity or imbalanced classes can be a very challenging task, especially in the medical imaging domain. In this paper, we propose a novel deep convolutional neural network, we called Self Supervised Super Sample Decomposition for Transfer learning (*4S-DT*) model. *4S-DT* encourages a coarse-to-fine transfer learning from large-scale image recognition tasks to a specific chest X-ray image classification task using a generic self-supervised sample decomposition approach. Our main contribution is a novel self-supervised learning mechanism guided by a super sample decomposition of unlabelled chest X-ray images. *4S-DT* helps in improving the robustness of knowledge transformation via a downstream learning strategy with a class-decomposition layer to simplify the local structure of the data. *4S-DT* can deal with any irregularities in the image dataset by investigating its class boundaries using a downstream class-decomposition mechanism. We used 50,000 unlabelled chest X-ray images to achieve our coarse-to-fine transfer learning with an application to COVID-19 detection, as an exemplar. *4S-DT* has achieved an accuracy of 97.54% in the detection of COVID-19 cases on an extended test set enriched by augmented images, out of which all real COVID-19 cases were detected, which was the highest accuracy obtained when compared to other methods.

Introduction

Diagnosis of COVID-19 is associated with the symptoms of pneumonia and chest X-ray tests¹. Chest X-ray is the essential imaging technique that plays an important role in the diagnosis of COVID-19 disease. Fig. 1 shows examples of a) a normal chest X-ray, a positive one with COVID-19, a positive image with the severe acute respiratory syndrome (SARS), and b) some examples of other unlabelled chest X-ray images used in this work.

Several statistical machine learning methods have been previously used for automatic classification of digitised lung

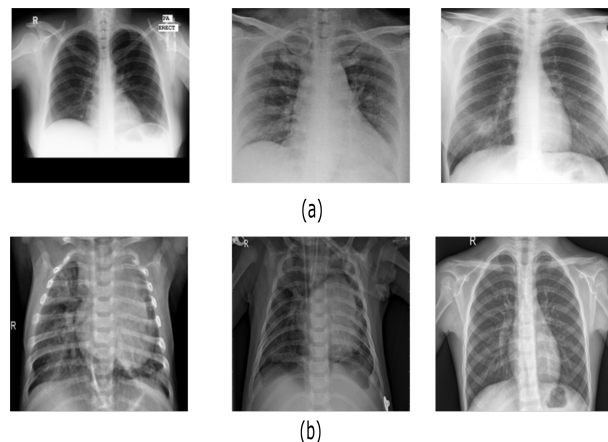


Figure 1. Examples of a) labelled chest X-ray images (from left to right: normal, COVID-19, and SARS images), and b) unlabelled chest X-ray images used in this work for self-supervision learning.

images^{2,3}. For instance, in⁴, a small set of three statistical features were calculated from lung texture to distinguish between malignant and benign lung nodules using a Support Vector Machine *SVM* classifier. A statistical co-occurrence matrix method was used with Backpropagation Network⁵ to classify samples from being normal or cancerous. With the high availability of enough annotated image data, deep learning approaches⁶⁻⁸ usually provide a superiority performance over the statistical machine learning approaches. Convolutional Neural Networks (*CNN*) is one of the most commonly used deep learning approaches with superior achievements in the medical imaging domain⁹. The primary success of *CNN* is due to its capability to learn local features automatically from domain-specific images, unlike the statistical machine learning methods. One of the popular strategies for training a *CNN* model is to transfer learned knowledge from a pre-trained network that fulfilled one generic task into a new specific task¹⁰. Transfer learning is faster and easy to apply without the need for a huge annotated dataset for training; therefore many scientists tend to adopt this strategy especially with medical imaging. Transfer learning can be accomplished with three main scenarios¹¹: a) “shallow tuning”, which adapts only the classification layer in a way to cope with the new task, and freezes the weights of the remaining layers without updating; b) “deep tuning” which aims to retrain all the weights of the adopted pre-trained network from end-to-end; and (c) “fine-tuning” that aims to gradually train layers by tuning the learning parameters until a significant performance boost is achieved. Transfer knowledge via fine-tuning scenario demonstrated outstanding performance in chest X-ray and computed tomography image classification^{12,13}.

The emergence of COVID-19 as a pandemic disease dictated the need for faster detection methods to contain the spread of the virus. As aforementioned, chest X-ray imaging comes in as a promising solution, particularly when combined with an effective machine learning model. In addition to data irregularities that can be dealt with through class decomposition, scarcity of data, especially in the early months of the pandemic, made it hard to realise the adoption of chest X-ray images as a means for detection. On the other hand, self-supervised learning is being popularised recently to address the expensive labelling of data acquired at an unprecedented rate. In self-supervised learning, unlabelled data is used for feature learning by assigning each example a pseudo label. In the case of convolutional neural networks (*CNN*) applied on image data, each image is assigned a pseudo label, and *CNN* is trained to extract visual features of the data. The training of a *CNN* by pseudo labelled images as input is called pretext task learning. While the training of the produced *CNN* from the pretext training using labelled data is called downstream task training. Inherently such a pipeline allows for effective utilisation of large unlabelled data sets. The success of the pretext task learning relies on pseudo labelling methods. In¹⁴, four categories of methods were identified. Context-based image feature learning by means of context similarity has demonstrated a particularly effective pseudo labelling mechanism. DeepCluster¹⁵ is the state-of-the-art method under this category. DeepCluster is a super sample decomposition method that generates pseudo labels through the clustering of *CNN* features. Sample decomposition is the process of applying clustering on the whole training set as a step for improving supervised learning performance¹⁶. When the clustering is performed on a larger data sample, we refer to this process as a super sample decomposition. However, we argue that the coupling of the pretext task and the pseudo labelling can limit the effectiveness of the pretext task in the self-supervised learning process. In our proposed super sample decomposition, the pretext task training uses cluster assignments as pseudo labels, where the clustering process is decoupled from the pretext training. We propose the clustering of encoded images through an auto-encoder neural network, allowing flexibility of utilising different features and clustering methods, as appropriate. We argue that this can be most effective in medical image classification, evident by the experimentally validated use of class decomposition for transfer learning in a method coined as DeTraC¹⁷.

In this paper, we propose a novel deep convolutional neural network, we term Self Supervised Super Sample Decomposition for Transfer learning (*4S-DT*) model for the detection of COVID-19 cases¹. *4S-DT* has been designed in a way to encourage a coarse-to-fine transfer learning based on a self-supervised sample decomposition approach. *4S-DT* can deal with any irregularities in the data distribution and the limited availability of training samples in some classes. The contributions of this paper can be summarised as follows. We provide

- a novel mechanism for self-supervised sample decomposition using a large set of unlabelled chest X-ray images for a pretext training task;
- a generic coarse-to-fine transfer learning strategy to gradually improve the robustness of knowledge transformation from large-scale image recognition tasks to a specific chest X-ray image classification task;
- a downstream class-decomposition layer in the downstream training phase to cope with any irregularities in the data distribution and simplify its local structure; and
- a thorough experimental study on COVID-19 detection, pushing the boundaries of state-of-the-art techniques in terms of accuracy, and robustness of the proposed model.

¹The developed code in a test mode is available at <https://github.com/asmaa4may/4S-DT>.

The paper is organised as follow. In Section , we review the state-of-the-art methods for COVID-19 detection. Section discusses the main components of our proposed *4S-DT* model. Section describes our experiments on several chest X-ray images collected from different hospitals. In Section , we discuss our findings and conclude the work.

Previous work on COVID-19 detection from chest X-ray

In February 2020, the World Health Organisation (WHO) has declared that a new virus called COVID-19 has started to spread aggressively in several countries¹⁸. Diagnosis of COVID-19 is typically associated with pneumonia-like symptoms, which can be revealed by both genetic and imaging tests. Fast detection of the virus will directly contribute to managing and controlling its spread. Imaging tests, especially chest X-ray, can provide fast detection of COVID-19 cases. The historical conception of medical image diagnostic systems has been comprehensively explored through an enormous number of approaches ranging from statistical machine learning to deep learning. A convolutional neural network is one of the most effective approaches in the diagnosis of lung diseases including COVID-19 directly from chest X-ray images. Several recent reviews have been carried out to highlight significant contributions to the detection of COVID-19¹⁹⁻²¹. For instance, in²², a modified version of ResNet-50 pre-trained *CNN* model has been used to classify *CT* images into three classes: healthy, COVID-19 and bacterial pneumonia. In²³, a *CNN* model, called COVID-Net, based on transfer learning was used to classify chest X-ray images into four classes: normal, bacterial infection, non-COVID, and COVID-19 viral infection. In²⁴, a weakly-supervised approach has been proposed using 3D chest CT volumes for COVID-19 detection and lesion localisation relying on ground truth masks obtained by an unsupervised lung segmentation method and a 3D ResNet pre-trained model. In²⁵, a dataset of chest X-ray images from patients with pneumonia, confirmed COVID-19 disease, and normal incidents, was used to evaluate the performance of the state-of-the-art *CNN* models based on transfer learning. The study suggested that transfer learning can provide important biomarkers for the detection of COVID-19 cases. It has been experimentally demonstrated that transfer learning can provide a robust solution to cope with the limited availability of training samples from confirmed COVID-19 cases²⁶.

In²⁷, self-supervised learning using context distortion is applied for classification, segmentation, and localisation in different medical imaging problems. When used in classification, the method was applied for scan plane detection in fetal 2D ultrasound images, showing classification improvement in some settings. However, we argue that our proposed method is more effective in image segmentation and localisation, because context distortion is able to generate localised features, instead of global image features that can be more effective for classification tasks.

Having reviewed the related work, it is evident that despite the great success of deep learning in the detection of COVID-19 cases from chest X-ray images, data scarcity and irregularities have not been explored. It is common in medical imaging in particular that datasets exhibit different types of irregularities (e.g. overlapping classes with imbalance problems) that affect the resulting accuracy of deep learning models. With the unfolding of COVID-19, chest X-ray images are rather scarce. Thus, this work focuses on coping with data irregularities through class decomposition, and data scarcity through super sample decomposition, as detailed in the following section.

4S-DT model

This section describes, in sufficient details, our proposed deep convolutional neural network, Self Supervised Super Sample Decomposition for Transfer learning (*4S-DT*) model for detecting COVID-19 cases from chest X-ray images. Starting with an overview of the architecture through to the different components of the model, the section discusses the workflow and formalises the method. *4S-DT* model consists of three training phases, see Fig. 2. In the first phase, we train an autoencoder model to extract deep local features from each sample in a super large set of unlabelled generic chest X-ray images. Then we adapted a sample decomposition mechanism to create pseudo labels for the generic chest X-ray images. In the second phase, we use the pseudo labels to achieve a coarse transfer learning using an ImageNet pre-trained *CNN* model for the classification of pseudo-labelled chest X-ray images (as a pretext training task), resulting in a chest X-ray-related convolutional features. In the last phase, we use trained convolutional features to achieve downstream training. The downstream training task is more task-specific by adapting a fine transfer learning from chest X-ray recognition to COVID-19 detection. In this stage, we also adapt a class-decomposition layer to simplify the local structure of the image data distribution, where a sophisticated gradient descent optimisation method is used. Finally, we apply a class-composition to refine the final classification of the images.

Super sample decomposition

Given a set of unlabelled images $X = \{x^1, x^2, \dots, x^n\}$, our super sample decomposition component aims to find and use pseudo labels during the pretext training task of *4S-DT*. To this end, an autoencoder (*AE*) is first used to extract deep features associated

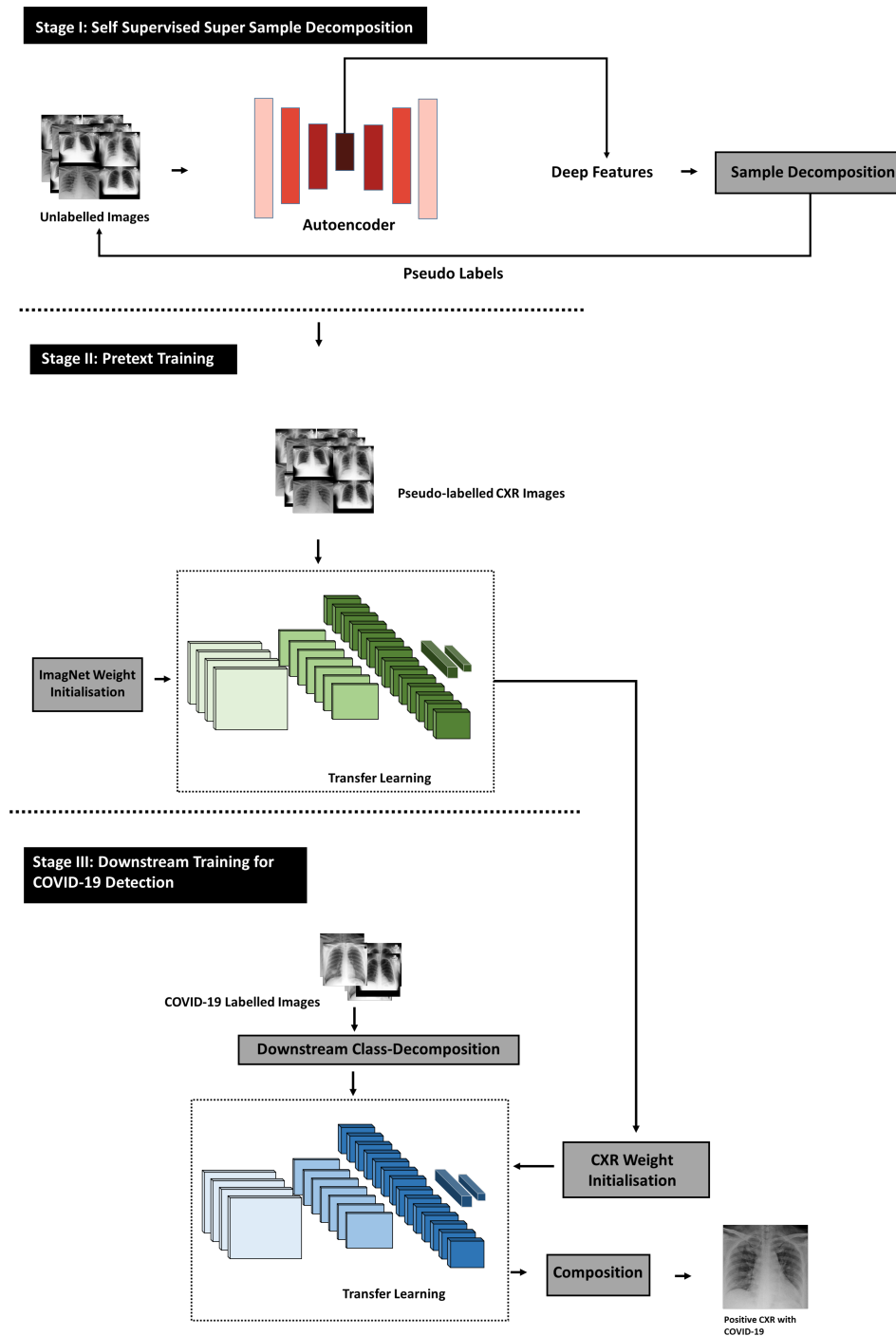


Figure 2. Graphical representation of *4S-DT* model.

to each image. For each input image x , the representation vector h^d and the reconstructed image \hat{x} can be defined as

$$h^d = f(W^{(1)}x + b^{(1)}) \quad (1)$$

$$\hat{x} = f(W^{(2)}h^d + b^{(2)}) \quad (2)$$

where $W^{(1)}$ and $W^{(2)}$ are the weight matrices, $b^{(1)}$ and $b^{(2)}$ are the bias vectors, and f is the active function. The reconstruction error $L(x, \hat{x})$ between \hat{x} and x is defined as

$$L(x, \hat{x}) = \frac{1}{2} \|x - \hat{x}\|^2 \quad (3)$$

The overall cost function of the n' unlabelled images, $E_{AE}(W, b)$, can be defined as

$$E_{AE}(W, b) = \left[\frac{1}{n'} \sum_{i=1}^{n'} L(x^i, \hat{x}^i) \right] + \frac{\lambda}{2} \sum_{l=1}^{n_l-1} \sum_{i=1}^{s_l} \sum_{j=1}^{s_{l+1}} (W_{ji}^{(l)})^2 \quad (4)$$

where the first term denotes the reconstruction error of the whole datasets, and the second term is the regularisation weight penalty term, which aims to prevent over-fitting by restraining the magnitude of the weights. λ is the weight decay parameter, n_l is the layer number of the network, s_l denotes the neuron number in layer l , and $W_{ji}^{(l)}$ is the connecting weight between neuron i in layer $l + 1$ and neuron j in layer l .

Once the training of the *AE* has been accomplished, Density-Based Spatial Clustering of Applications with Noise (*DBSCAN*) is used to cluster the image data distribution X into a number of classes c based on the extracted features h^d . *DBSCAN* is an unsupervised clustering algorithm, which is a considerably representative density-based clustering algorithm that defines clusters as the largest set of points connected by density.

Let the image dataset X be mapped into a low-dimensional feature space denoted by $H \in \mathbb{R}^{n' \times d}$, where $H = (h_1, h_2, \dots, h_{n'})$. An image x^i (represented by h_i) is density-connected to image x^j (represented by h_j) with respect to *Eps* (i.e. neighbourhood radius) and *MinPts* (i.e. the minimum number of objects within the neighbourhood radius of core object) if there exists a core object x^k such that both x^i and x^j are directly density-reachable from x^k with respect to *Eps* and *MinPts*. An image x^i is directly density-reachable from an image x^j if x^i is within the *Eps*-neighbourhood of $N_{Eps}(x^j)$, and x^j is a core object, where *Eps*-neighbourhood can be defined as

$$N_{Eps}(x_j) = \{x_i \in X | dis(x_i, x_j) \leq Eps\}. \quad (5)$$

DBSCAN results in C clusters, where each cluster is constructed by maximising the density reachability relationship among images of the same cluster. The C cluster labels will be assigned to the n' unlabelled images and will be presented as pseudo labels for the pretext training task and hence the downstream training task. The pseudo-labelled image dataset can then be defined as $X' = \{(x^i, y^c) | c \in C\}$.

Pretext training

With the high availability of large-scale annotated image datasets, the chance for the different classes to be well-represented is high. Therefore, the learned in-between class-boundaries are most likely to be generic enough to new samples. On the other hand, with the limited availability of annotated medical image data, especially when some classes are suffering more compared to others in terms of the size and representation, the generalisation error might increase. This is because there might be a miscalibration between the minority and majority classes. Large-scale annotated image datasets (such as ImageNet) provide effective solutions to such a challenge via transfer learning where tens of millions of parameters (of *CNN* architectures) are required to be trained.

A shallow-tuning mode was used during the adaptation and training of an ImageNet pre-trained *CNN* model using the collected chest X-ray image dataset. We used the off-the-shelf *CNN* features of pre-trained models on ImageNet (where the training is accomplished only on the final classification layer) to construct the image feature space.

Mini-batch of stochastic gradient descent (*mSGD*) was used to minimise the categorical cross entropy loss function, $E_{coarse}(\cdot)$

$$E_{coarse}(y^c, z'(x^j, W')) = - \sum_{c=1}^C y^c \ln z'(x^j, W'), \quad (6)$$

where x^j is the set of self-labelled images in the training, y^c is their associated self labels while $z'(x^j, W')$ is the predicted output from a softmax function, where W' is the converged weight matrix associated to the ImageNet pre-trained model (i.e. we used W' of ImageNet pre-trained CNN model for weight initialisation to achieve a coarse transfer learning).

Downstream training

A fine-tuning mode was used during the adaptation of *ResNet* model using feature maps from the coarse transfer learning stage. However, due to the high dimensionality associated with the images, we applied *PCA* to project the high-dimension feature space into a lower-dimension, where highly correlated features were ignored. This step is important for the downstream class-decomposition process in the downstream training phase to produce more homogeneous classes, reduce the memory requirements, and improve the efficiency of the framework.

Now assume that our feature space (*PCA*'s output) is represented by a 2-D matrix (denoted as dataset A), and \mathbf{L} is a class category. A and \mathbf{L} can be rewritten as

$$A = \begin{bmatrix} a_{11} & a_{11} & \dots & a_{1m} \\ a_{21} & a_{22} & \dots & a_{2m} \\ \vdots & \vdots & \vdots & \vdots \\ a_{n1} & a_{n2} & \dots & a_{nm} \end{bmatrix}, \mathbf{L} = \{l_1, l_2, \dots, l_{c'}\}, \quad (7)$$

where n is the number of images, m is the number of features, and c' is the number of classes. For downstream class-decomposition, we used k -means clustering²⁸ to further divide each class into homogeneous sub-classes (or clusters), where each pattern in the original class \mathbf{L} is assigned to a class label associated with the nearest centroid based on the squared euclidean distance (*SED*):

$$SED = \sum_{j=1}^k \sum_{i=1}^n \| a_i^{(j)} - c_j \|^2, \quad (8)$$

where centroids are denoted as c_j . Once the clustering is accomplished, each class in \mathbf{L} will further be divided into k subclasses, resulting in a new dataset (denoted as dataset B). Accordingly, the relationship between dataset A and B can be mathematically described as:

$$A = (A|\mathbf{L}) \mapsto B = (B|\mathbf{C}') \quad (9)$$

where the number of instances in A is equal to B while \mathbf{C}' encodes the new labels of the subclasses (e.g. $\mathbf{C}' = \{l_{11}, l_{12}, \dots, l_{1k}, l_{21}, l_{22}, \dots, l_{2k}, \dots, l_{c'k}\}$).

For transfer learning, we used ResNet²⁹ model, which showed excellent performance with only 18 layers. Here we consider freezing the weights of low-level layers and update weights of high-level layers. With the limited availability of training data, stochastic gradient descent (SGD) can heavily be fluctuating the objective/loss function and hence overfitting can occur. To improve convergence and overcome overfitting, the mini-batch of stochastic gradient descent (*mSGD*) was used to minimise the objective function, $E_{fine}(\cdot)$, with categorical cross-entropy loss

$$E_{fine}(g^{l^i}, z(o^j, \hat{W})) = - \sum_{i=1}^{c'k} g^{l^i} \ln z(o^j, \hat{W}), \quad (10)$$

where o^j is the set of input labelled images in the training, g^{l^i} is the ground truth labels, while $z(o^j, \hat{W})$ is the predicted output from a softmax function, where \hat{W} is the converged weight matrix associated to the coarse transfer learning model.

Performance evaluation

In the downstream class-decomposition layer of *4S-DT*, we divide each class within the image dataset into several sub-classes, where each subclass is treated as a new independent class. In the composition phase, those sub-classes are assembled back to produce the final prediction based on the original image dataset. For performance evaluation, we adopted Accuracy (ACC), Specificity (SP) and Sensitivity (SN) metrics for multi-classes confusion matrix, the input image can be classified into one of (c') non-overlapping classes. As a consequence, the confusion matrix would be a ($N_{c'} \times N_{c'}$) matrix and the matrices are defined as:

$$\text{Accuracy}(ACC) = \frac{1}{c'} \sum_{i=1}^{c'} \frac{TP_i + TN_i}{TP_i + TN_i + FP_i + FN_i}, \quad (11)$$

$$\text{Sensitivity}(SN) = \frac{1}{c'} \sum_{i=1}^{c'} \frac{TP_i}{TP_i + FN_i}, \quad (12)$$

$$\text{Specificity}(SP) = \frac{1}{c'} \sum_{i=1}^{c'} \frac{TN_i}{TN_i + FP_i}, \quad (13)$$

where c' is the original number of classes in the dataset, TP is the true positive in case of COVID-19 case and TN is the true negative in case of normal or other disease, while FP and FN are the incorrect model predictions for COVID-19 and other cases. Also, the TP , TN , FP and FN for a specific class i are defined as:

$$TP_i = \sum_{i=1}^n x_{ii} \quad (14)$$

$$TN_i = \sum_{j=1}^c \sum_{k=1}^c x_{jk}, j \neq i, k \neq i \quad (15)$$

$$FP_i = \sum_{j=1}^c x_{ji}, j \neq i \quad (16)$$

$$FN_i = \sum_{j=1}^c x_{ij}, j \neq i, \quad (17)$$

where x_{ii} is an element in the diagonal of the matrix. Having discussed and formalised the *4S-DT* model in this section in detail, the following section validates the model experimentally. The model establishes the effectiveness of self-supervised super sample decomposition in detecting COVID-19 from chest X-ray images.

Results

This section presents the datasets used in training and evaluating our *4S-DT* model, and discusses the experimental results.

Datasets

In this work, we used two datasets of labelled and unlabelled chest X-ray images, defined respectively as:

- **Unlabelled chest X-ray dataset**, a large set of chest X-ray images used as an unlabelled dataset: A set of 50,000 unlabelled chest X-ray images collected from three different datasets: 1) 336 cases with a manifestation of tuberculosis, and 326 normal cases from^{30,31}; 2) 5,863 chest X-Ray images with 2 categories: pneumonia and normal from³²; and 3) a set of 43,475 chest X-ray images randomly selected from a total of 112,120 chest X-ray images, including 14 diseases, available from³³.
- **COVID-19 dataset**, an imbalanced set of labelled chest X-ray with COVID-19 cases: 80 normal cases from^{34,35}, and chest X-ray dataset from³⁶, which contains 105 and 11 cases of COVID-19 and SARS, respectively. We divided the dataset into two groups: 70% for training and 30% for testing. Due to the limited availability of training images, we applied different data augmentation techniques (such as: flipping up/down and right/left, translation and rotation using random five different angles) to generate more samples, see Table 1.

All the experiments in our work have been carried out in MATLAB 2019a on a PC with the following configuration: 3.70 GHz Intel(R) Core(TM) i3-6100 Duo, NVIDIA Corporation with the donation of the Quadro P5000GPU, and 8.00 GB RAM.

Self supervised training of *4S-DT*

We trained our autoencoder with 80 neurons in the first hidden layer and 50 neurons in the second hidden layer for the reconstruction of input unlabelled images, see Fig 3. The trained autoencoder is then used to extract a set of deep features from the unlabelled chest X-ray images. The extracted features were fed into the *DBSCAN* clustering algorithm for constructing the

Table 1. The distribution of original classes in labelled images

Type	COVID-19	SARS	Normal	Total
Training set	74	8	56	138
Augmented training set	662	69	504	1235
Testing set 1	31	3	24	58
Testing set 2	283	30	216	529



(a) original image

(b) reconstructed image

Figure 3. An example of a reconstructed chest X-ray image by our Autoencoder.

clusters (and hence the pseudo-labels). Since *DBSCAN* is sensitive to the neighbourhood radius, we employed a *k*-nearest-neighbour (*k*-*NN*)³⁷ search to determine the optimal (*Eps*) value. As demonstrated in Fig 4, the optimal value for *Eps* was 1.861. *MinPts* parameter has been derived from the number of features (*d*) such that $MinPts \geq d + 1$. Consequently, we used and tested different values for *MinPts* parameter such as 51, 54, and 56 resulting in 13, 6, and 4 clusters respectively. For the coarse transfer learning, we used ResNet18 pre-trained *CNN* model. The classification performance, on the pseudo-labelled samples, associated with the 13, 6, and 4 clusters were 48.1%, 53.26%, and 64.37%, respectively. Therefore, we fix the number of clusters (and hence the number of pseudo labels) to be 4 in all experiments in this work.

Downstream class-decomposition of 4S-DT

We used AlexNet³⁸ pre-trained network based on a shallow learning mode to extract discriminative features of the labelled dataset. We set a value of 0.0001 for the learning rate, except the last fully connected layer (was 0.01), the min-batch size was 128 with the minimum of 256 epochs, 0.001 was set for the weight decay to prevent the overfitting through training the model, and 0.9 for the momentum speed. At this stage, 4096 attributes were obtained, therefore we used *PCA* to reduce the dimension of feature space. We found that the first 53, 8, and 43 components for COVID-19, SARS, and normal, respectively, explain more than threshold= 95% variability. For the class decomposition step, we used *k*-means clustering²⁸, where *k* has been selected to be 2 and hence each class in **L** has been further divided into two subclasses, resulting in a new dataset with six classes. The adoption of *k*-means for class decomposition with $k = 2$ is based on the results achieved by the DeTraC model in¹⁷.

Classification performance on COVID-19 dataset

We first validate the performance of 4S-DT with ResNet18 (as the backbone network) on the 58 test images (i.e. testing set 1), where augmented training set is used for training, see Table 1. Our ResNet architecture consists of residual blocks and each block has two 3×3 *Conv* layers, where each layer is followed by batch normalisation and a ReLU activation function. Our ResNet architecture consists of residual blocks and each block has two 3×3 *Conv* layers, where each layer is followed by batch

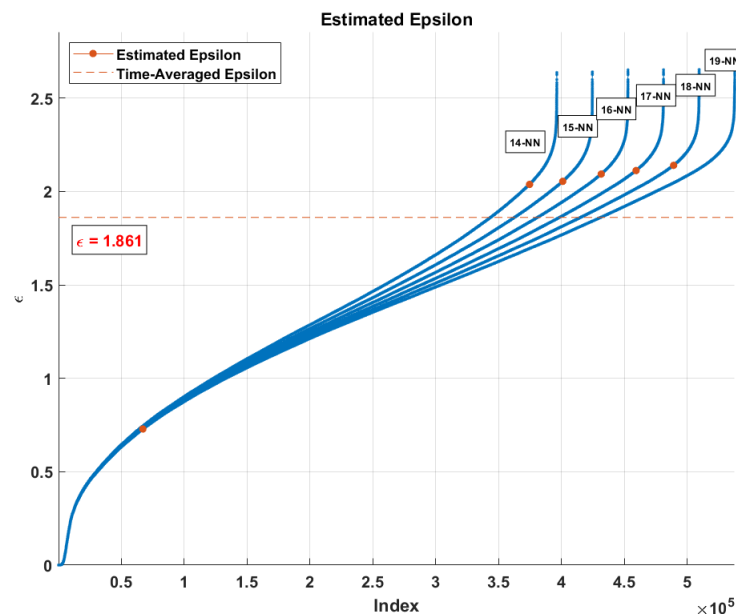


Figure 4. Estimation of the optimal Eps .

Table 2. The adopted ResNet architecture used in the fine-tuning study in our experiments.

Layer Name	ResNet_18	Output Size
Conv1	7×7 , 64, stride (2)	$112 \times 112 \times 64$
Conv2	Layer-Res2a Layer-Res2b	$56 \times 56 \times 64$
Conv3	Layer-Res3a Layer-Res3b	$28 \times 28 \times 128$
Conv4	Layer-Res4a Layer-Res4b	$14 \times 14 \times 256$
Conv5	Layer-Res5a Layer-Res5b	$7 \times 7 \times 512$

normalisation and a ReLU activation function. Table 2 illustrates the adopted architecture used in our experiment.

During the training of the backbone network, the learning rate for all the *CNN* layers was fixed to 0.0001 except for the last fully connected layer (was 0.01) to accelerate the learning. The mini-batch size was 256 with a minimum of 200 epochs, 0.0001 was set for the weight decay to prevent the overfitting through training the model, and the momentum value was 0.95. The schedule of drop learning rate was set to 0.95 every 5 epochs. The results were summarised in Table 4. Moreover, we also compare the performance of the proposed model without the self supervised sample decomposition component (i.e. w/o *4S-D* or *DeTraC-ResNet18*¹⁷) and without both *4S-D* and class-decomposition (w/o *4S-D+CD* or ResNet18²⁹ pre-trained network on) the 58 testing set. *4S-DT* has achieved 100% accuracy in the detection of COVID-19 cases, see Fig. 5. As illustrated by Fig. 5 and Table 3, *4S-DT* shows a superiority and a significant contribution in improving the transfer learning process with both the self supervised sample decomposition and downstream class-decomposition components. To further investigate the robustness of *4S-DT*, we trained *4S-DT* on the augmented images only and tested its performance on the 196 original cases. *4S-DT* has achieved 96.43% accuracy in the detection of COVID-19 cases with sensitivity of 97.1% and specificity of 95.60 %, see in Fig. 5.

To allow for further investigation and make testing of COVID-19 detection more challenging, we applied the same data augmentation techniques (used for the training samples) to the small testing set to increase the number of testing samples. The new test sample distribution, we called testing set 2, contains 283 COVID-19 images, 30 SARS images, and 216 normal images, see Table 1. Consequently, we used testing set 2 for testing and augmented training set for training (see Table 1), unless otherwise mentioned, for the performance evaluation of all methods in the experiments described below. We validated the

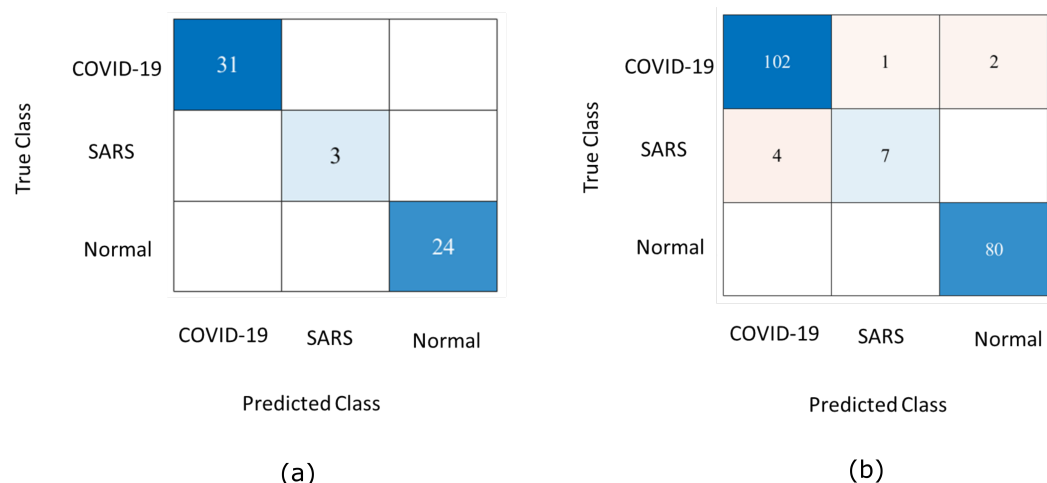


Figure 5. Confusion matrix obtained by a) *4S-DT* on the 58 test set, and b) *4S-DT* when trained on augmented images only and tested on the 196 cases.

Table 3. Classification measurements obtained by *4S-DT* without ResNet and without both *4S-D* and class-decomposition (w/o *4S-D+CD*) and without *4S-D* (w/o *4S-D*) only on the 58 labelled chest X-ray images (i.e. testing set 1).

(w/o <i>4S-D+CD</i>)			(w/o <i>4S-D</i>)		
ACC (%)	SN (%)	SP (%)	ACC (%)	SN (%)	SP (%)
89.66%	96.77%	81.48%	93.10%	96.77%	88.89%

performance of a) the full version of *4S-DT* with *4S-D* component and b) without *4S-D*. For a fair comparison, we used the same backbone network (i.e. ResNet18) with the downstream class-decomposition component, where both versions have been trained in a shallow and fine-tuning mode. As illustrated by Table 4, *4S-D* component shows significant improvement in shallow- and fine-tuning modes in all cases. More importantly, our full version model with *4S-D* demonstrates better performance, in each case, with less number of epochs, confirming its efficiency and robustness at the same time.

Moreover, we compared the classification performance of *4S-DT* with other models used for COVID-19 detection, including GoogleNet³⁹, *DeTraC*. As shown by Table 5, *4S-DT* has demonstrated superiority in performance, confirming its effectiveness in improving the classification accuracy of transfer learning models. Finally, Fig. 6 shows the Area Under the receiver curve (AUC) between the true positive rate and false positive rate obtained by *4S-DT* to confirm its robustness behaviours during the training process.

Table 4. Overall classification performance of *4S-DT* model with and without self-supervised sample decomposition (*4S-D*) component, on testing set 2.

Layer	without <i>4S-D</i>				with <i>4S-D</i>			
	ACC (%)	SN (%)	SP (%)	Epochs #	ACC (%)	SN (%)	SP (%)	Epochs #
Shallow	92.12	64.13	94.2	61	97.48	88.64	98.01	29
Res5b	93.84	64.18	94.06	75	97.66	93.08	98.41	42
Res5a	93.84	64.18	94.06	83	97.23	87.33	97.73	33
Res4b	93.96	64.33	94.20	112	96.8	86.3	97.91	32
Res4a	94.04	64.52	94.37	82	97.99	87.15	98.10	25
Res3b	94.34	64.16	94.25	73	97.99	87.71	97.42	32

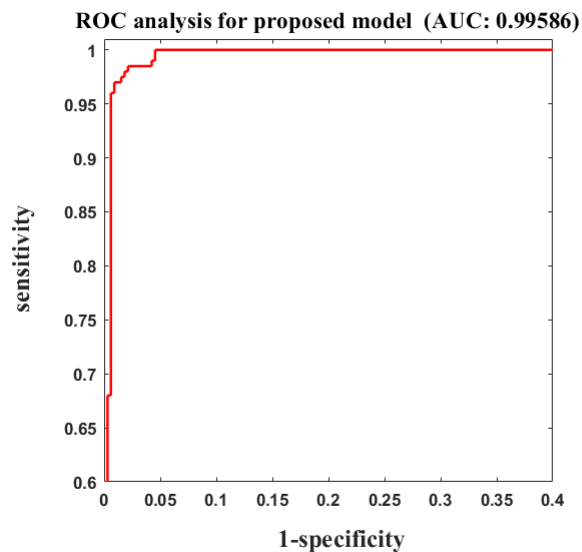


Figure 6. ROC curve obtained during the training of *4S-DT* with ResNet pre-trained model.

Table 5. Classification performance of *4S-DT* and other models on testing set 2 of the COVID-19 dataset.

Model	ACC (%)	SN (%)	SP (%)
<i>4S-DT</i> (ResNet)	97.54	97.88	97.15
<i>4S-DT</i> (GoogleNet)	94.15	97.07	93.08
<i>4S-DT</i> (Vgg19)	95.28	93.66	97.15
<i>DeTraC-ResNet18</i> ⁴⁰	95.12	97.91	91.87
ResNet18 ²⁹	92.5	65.01	94.3
<i>DeTraC-GoogleNet</i> ⁴⁰	91.01	76.03	82.6
<i>DeTraC-Vgg19</i> ⁴⁰	93.42	89.71	95.7

Discussion

The diagnosis of COVID-19 is associated with the pneumonia-like symptoms that can be revealed by genetic and imaging tests. Chest X-ray imaging test provides a promising fast detection of COVID-19 cases and consequently can contribute to controlling the spread of the virus. In medical image classification, paramount progress has been made using ImageNet pre-trained convolutional neural networks (CNNs), exploiting the high availability of large-scale annotated image datasets. The historical conception of such approaches has been comprehensively explored through several transfer learning strategies, including fine-tuning and deep-tuning mechanisms. They usually require an enormous number of balanced annotated images distributed over several classes/diseases (which is impractical in the medical imaging domain). In medical image analysis, data irregularities still remain a challenging problem, especially with the limited availability of confirmed samples with some diseases such as COVID-19 and SARS, which usually results in miscalibration between the different classes in the dataset. Consequently, COVID-19 detection from chest X-ray images presents a challenging problem due to the irregularities and the limited availability of annotated cases.

Here, we propose a new CNN model, we called Self Supervised Super Sample Decomposition for Transfer learning (4S-DT) model. 4S-DT has been designed to cope with such challenging problems by adapting a self-supervised sample decomposition approach to generate pseudo-labels for the classification of unlabelled chest X-ray images as a pretext learning task. 4S-DT has also the ability to deal with data irregularities by a class-decomposition adapted in its downstream learning component. 4S-DT has demonstrated its effectiveness and efficiency in coping with the detection of COVID-19 cases in a dataset with irregularities in its distribution. In this work, we used 50,000 unlabelled chest X-ray images for the development of our self-supervised sample decomposition approach to perform transfer learning with an application to COVID-19 detection. We achieved an accuracy of 97.54% with a specificity of 97.15% and sensitivity of 97.88% on 529 test chest X-ray images, i.e. testing set 2, with 283 COVID-19 samples. We also achieved 100% accuracy in the detection of COVID-19 cases in a small test dataset, testing set 1, of 58 cases, including 31 COVID-19 cases.

With the continuous collection of data, we aim in the future to extend the development and validation of 4S-DT with multi-modality datasets, including clinical records. As a future development, we also aim to add an explainability component to increase the trustworthiness and usability of 4S-DT. Finally, one can use model pruning and quantisation to improve the efficiency of 4S-DT, allowing deployment on handheld devices.

References

1. Shi, H. *et al.* Radiological findings from 81 patients with covid-19 pneumonia in wuhan, china: a descriptive study. *The Lancet Infect. Dis.* (2020).
2. Dandil, E. *et al.* Artificial neural network-based classification system for lung nodules on computed tomography scans. In *2014 6th International conference of soft computing and pattern recognition (SoCPaR)*, 382–386 (IEEE, 2014).
3. Kuruvilla, J. & Gunavathi, K. Lung cancer classification using neural networks for ct images. *Comput. methods programs biomedicine* **113**, 202–209 (2014).
4. Manikandan, T. & Bharathi, N. Lung cancer detection using fuzzy auto-seed cluster means morphological segmentation and svm classifier. *J. medical systems* **40**, 181 (2016).
5. Sangamithraa, P. & Govindaraju, S. Lung tumour detection and classification using ek-mean clustering. In *2016 International Conference on Wireless Communications, Signal Processing and Networking (WiSPNET)*, 2201–2206 (IEEE, 2016).
6. Pesce, E. *et al.* Learning to detect chest radiographs containing pulmonary lesions using visual attention networks. *Med. Image Analysis* **53**, 26 – 38 (2019).
7. Xie, Y., Zhang, J. & Xia, Y. Semi-supervised adversarial model for benign–malignant lung nodule classification on chest ct. *Med. Image Analysis* **57**, 237 – 248 (2019).
8. Abbas, A. & Abdelsamea, M. M. Learning transformations for automated classification of manifestation of tuberculosis using convolutional neural network. In *2018 13th IEEE International Conference on Computer Engineering and Systems (ICCES)*, 122–126, DOI: [10.1109/ICCES.2018.8639200](https://doi.org/10.1109/ICCES.2018.8639200) (2018).
9. LeCun, Y., Bengio, Y. & Hinton, G. Deep learning. *nature* **521**, 436 (2015).
10. Pan, S. J. & Yang, Q. A survey on transfer learning. *IEEE Transactions on knowledge data engineering* **22**, 1345–1359 (2009).
11. Li, Q. *et al.* Medical image classification with convolutional neural network. In *2014 13th International Conference on Control Automation Robotics & Vision (ICARCV)*, 844–848 (IEEE, 2014).

12. Joyseeree, R., Otálora, S., Müller, H. & Depeursinge, A. Fusing learned representations from riesz filters and deep cnn for lung tissue classification. *Med. Image Analysis* **56**, 172 – 183 (2019).
13. Gao, M. *et al.* Holistic classification of ct attenuation patterns for interstitial lung diseases via deep convolutional neural networks. *Comput. Methods Biomech. Biomed. Eng. Imaging & Vis.* **6**, 1–6 (2018).
14. Jing, L. & Tian, Y. Self-supervised visual feature learning with deep neural networks: A survey. *IEEE Transactions on Pattern Analysis Mach. Intell.* (2020).
15. Caron, M., Bojanowski, P., Joulin, A. & Douze, M. Deep clustering for unsupervised learning of visual features. In *Proceedings of the European Conference on Computer Vision (ECCV)*, 132–149 (2018).
16. Rokach, L., Maimon, O. & Arad, O. Improving supervised learning by sample decomposition. *Int. J. Comput. Intell. Appl.* **5**, 37–53 (2005).
17. Abbas, A., Abdelsamea, M. M. & Gaber, M. M. Detrac: Transfer learning of class decomposed medical images in convolutional neural networks. *IEEE Access* **8**, 74901–74913 (2020).
18. Organization, W. H. *et al.* Coronavirus disease 2019 (covid-19): situation report, 51. (2020).
19. Shi, F. *et al.* Review of artificial intelligence techniques in imaging data acquisition, segmentation and diagnosis for covid-19. *IEEE Rev. Biomed. Eng.* (2020).
20. Dong, D. *et al.* The role of imaging in the detection and management of covid-19: a review. *IEEE Rev. Biomed. Eng.* 1–1 (2020).
21. Li, L. *et al.* Artificial intelligence distinguishes covid-19 from community acquired pneumonia on chest ct. *Radiology* 200905 (2020).
22. Song, Y. *et al.* Deep learning enables accurate diagnosis of novel coronavirus (covid-19) with ct images. *medRxiv* (2020).
23. Wang, L. & Wong, A. Covid-net: A tailored deep convolutional neural network design for detection of covid-19 cases from chest radiography images (2020). [2003.09871](https://doi.org/10.26434/chemrxiv-2020-09871).
24. Wang, X. *et al.* A weakly-supervised framework for covid-19 classification and lesion localization from chest ct. *IEEE Transactions on Med. Imaging* 1–1 (2020).
25. Apostolopoulos, I. D. & Mpesiana, T. A. Covid-19: automatic detection from x-ray images utilizing transfer learning with convolutional neural networks. *Phys. Eng. Sci. Medicine* **1** (2020).
26. Oh, Y., Park, S. & Ye, J. C. Deep learning covid-19 features on cxr using limited training data sets. *IEEE Transactions on Med. Imaging* 1–1 (2020).
27. Chen, L. *et al.* Self-supervised learning for medical image analysis using image context restoration. *Med. image analysis* **58**, 101539 (2019).
28. Wu, X. *et al.* Top 10 algorithms in data mining. *Knowl. information systems* **14**, 1–37 (2008).
29. He, K., Zhang, X., Ren, S. & Sun, J. Deep residual learning for image recognition. In *Proceedings of the IEEE conference on computer vision and pattern recognition*, 770–778 (2016).
30. Jaeger, S. *et al.* Automatic tuberculosis screening using chest radiographs. *IEEE transactions on medical imaging* **33**, 233–245 (2013).
31. Candemir, S. *et al.* Lung segmentation in chest radiographs using anatomical atlases with nonrigid registration. *IEEE transactions on medical imaging* **33**, 577–590 (2013).
32. Kermany, D. S. *et al.* Identifying medical diagnoses and treatable diseases by image-based deep learning. *Cell* **172**, 1122–1131 (2018).
33. Wang, X. *et al.* Chestx-ray8: Hospital-scale chest x-ray database and benchmarks on weakly-supervised classification and localization of common thorax diseases. In *Proceedings of the IEEE conference on computer vision and pattern recognition*, 2097–2106 (2017).
34. Candemir, S. *et al.* Lung segmentation in chest radiographs using anatomical atlases with nonrigid registration. *IEEE Transactions on Med. Imaging* **33**, 577–590, DOI: [10.1109/TMI.2013.2290491](https://doi.org/10.1109/TMI.2013.2290491) (2014).
35. Jaeger, S. *et al.* Automatic tuberculosis screening using chest radiographs. *IEEE Transactions on Med. Imaging* **33**, 233–245, DOI: [10.1109/TMI.2013.2284099](https://doi.org/10.1109/TMI.2013.2284099) (2014).
36. Cohen, J. P., Morrison, P. & Dao, L. Covid-19 image data collection. *arXiv preprint arXiv:2003.11597* (2020).

37. Dudani, S. A. The distance-weighted k-nearest-neighbor rule. *IEEE Transactions on Syst. Man, Cybern.* 325–327 (1976).
38. Krizhevsky, A., Sutskever, I. & Hinton, G. E. Imagenet classification with deep convolutional neural networks. In *Advances in neural information processing systems*, 1097–1105 (2012).
39. Szegedy, C. *et al.* Going deeper with convolutions. In *Proceedings of the IEEE conference on computer vision and pattern recognition*, 1–9 (2015).
40. Abbas, A., Abdelsamea, M. M. & Gaber, M. M. Classification of covid-19 in chest x-ray images using detrac deep convolutional neural network. *arXiv preprint arXiv:2003.13815* (2020).